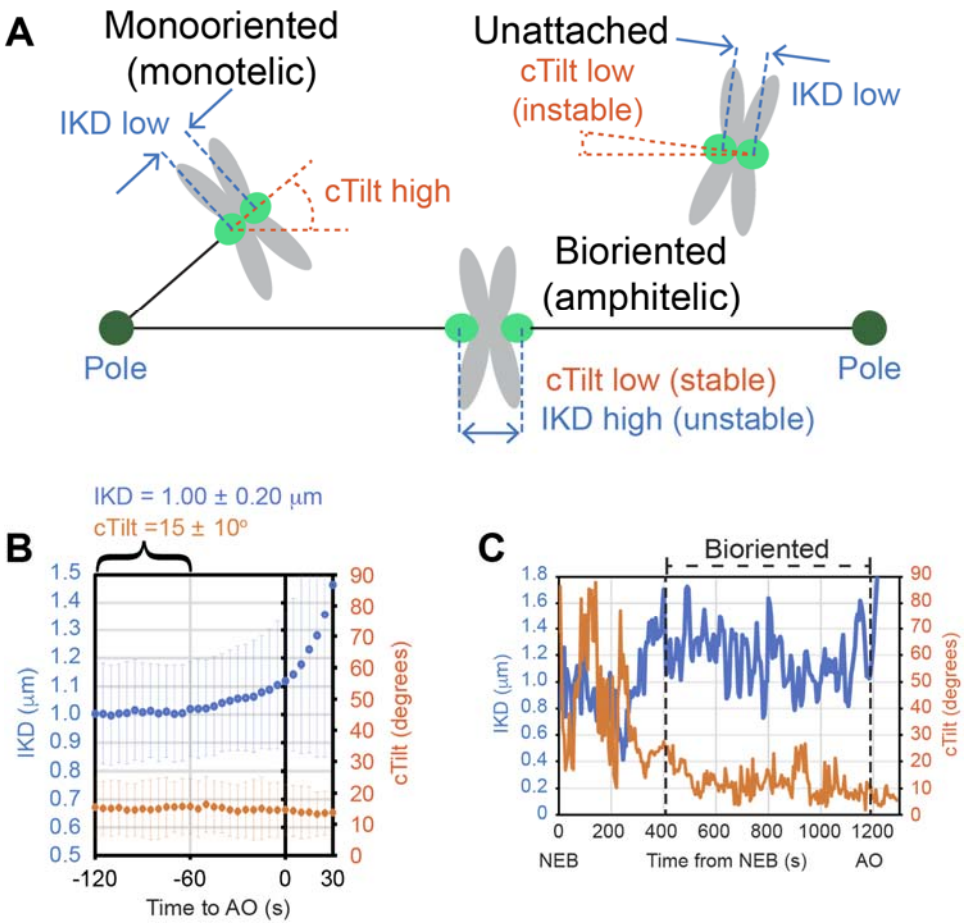

Figure S1. Criteria for detection of amphitelic attachments in centromere trajectories. Related to Figure 1. (A) Differences in the centromere orientation and stretching expected for unattached, monooriented, and bioriented chromosomes. Formation of amphitelic attachments leads to poleward pulling forces acting in the opposite directions on sister kinetochores. Thus, biorientation is manifested as an increase in interkinetochore distance (IKD) and a stable decrease of the angle between the centromere axis and spindle axis (centromere tilt, cTilt). **(B)** Mean values of IKD and cTilt observed in RPE1 cells during the two minutes prior to the onset of anaphase (AO) when all chromosomes have formed amphitelic attachments. Error bars are STD. **(C)** Dynamics of IKD and cTilt for a chromosome in RPE1 cell. Dashed lines denote timespan when the chromosome meets the biorientation criteria of IKD > 0.9 μm and cTilt < 22.5°. NEB, nuclear envelope breakdown.

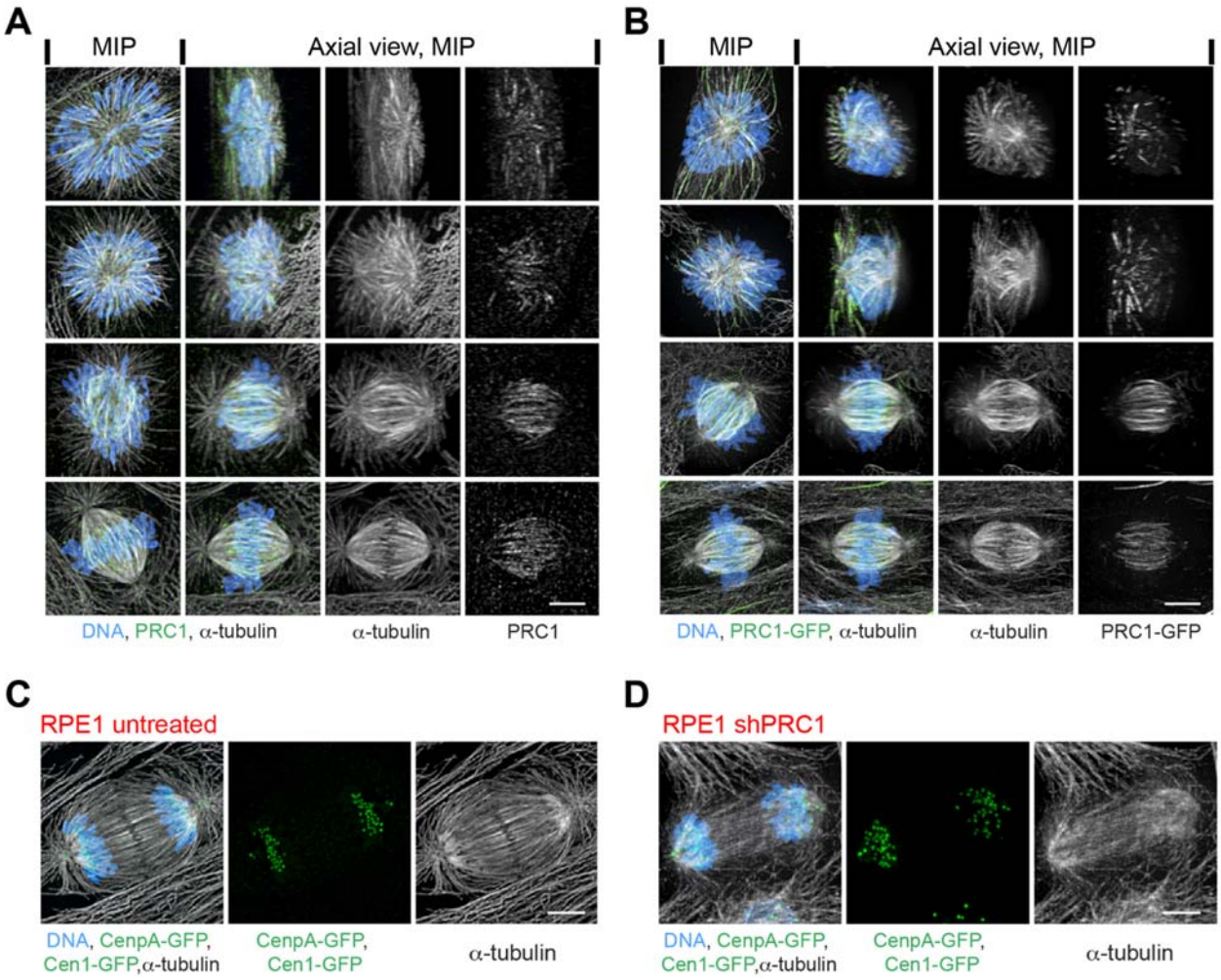

Figure S2. Distribution of PRC1 at various stages of mitosis and the effect of PRC1 depletion in RPE1 cells. Related to Figures 2 and 3. (A) Selected cells immuno-stained for microtubules (α-tubulin) and PRC1. Chromosomes are counterstained with Hoechst 33342. All images are maximal-intensity projections of 3-D volumes that include the entire cell. Left column presents cells in their natural orientation. Three right columns present the same volumes rotated to generate a precisely axial view of the spindle. Notice that PRC1-positive bundles form a barrel-shaped structure within the spindle. **(B)** Similar to (A) but the bundles are visualized via constitutive ectopic expression of full-length PRC1-GFP. Notice similarity in the distribution patterns of the endogenous PRC1 (A) and PRC1-GFP (B). **(C-D)** Spindle architecture during telophase in a wild-type RPE1 cell (C) vs. RPE1 cell depleted of PRC1 (D). Notice lack of microtubule bundles in the depleted cell. Timelapse recording of the cell shown in (D) is presented in Video S3 and selected frames from the recording – in Figure 3C. The cell was fixed within seconds after the last recorded timepoint and stained for α-Tubulin. Only cells that lacked microtubule bundles during telophase were selected for analyses of KT movements. Scale bars, 5 μm.

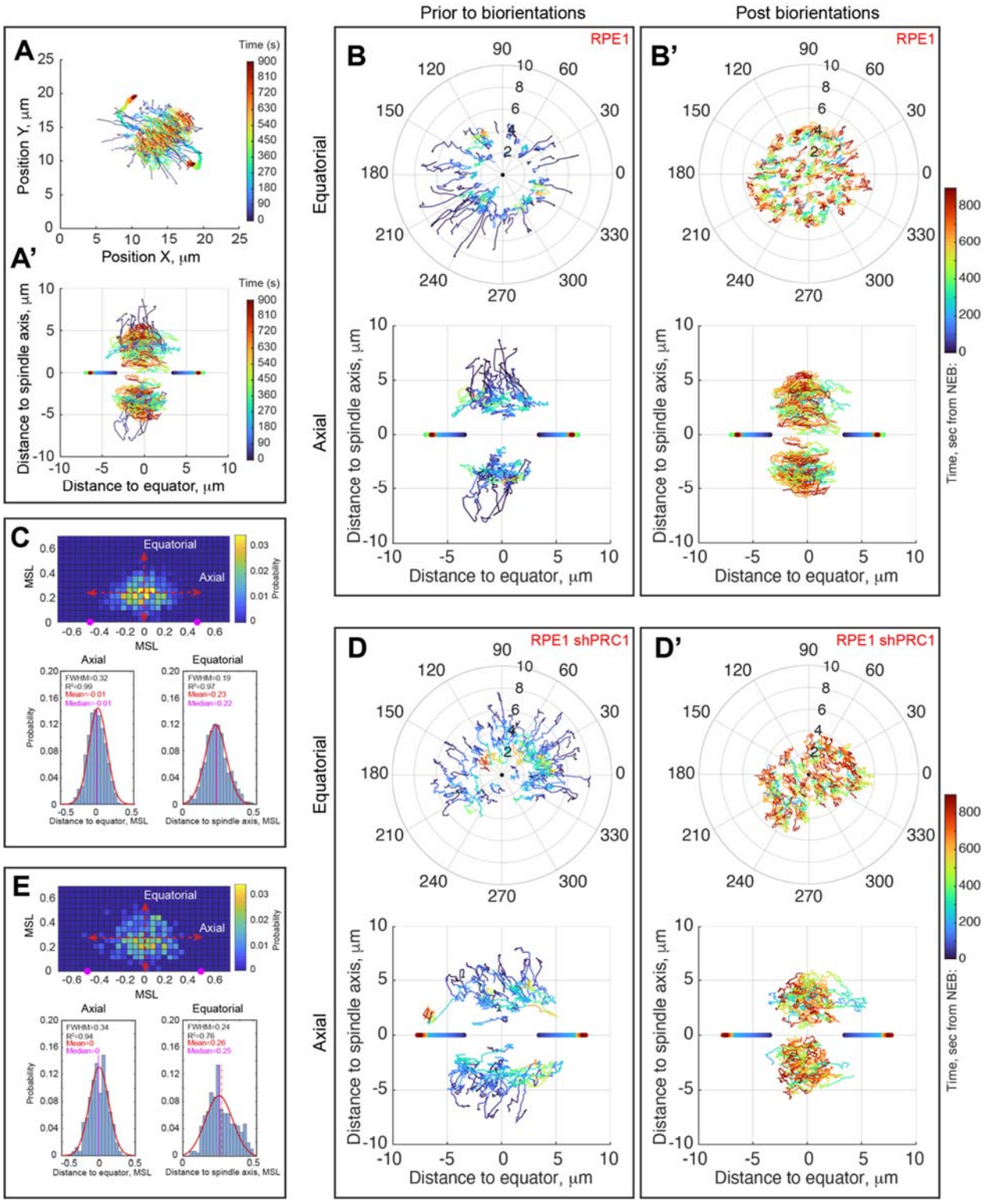

Figure S3. Methodology for analyses of centromere movements and spatial distribution of biorientation events. Related to Figure 3. (A) Trajectories of spindle poles (thicker lines) and centromeres (thinner lines) plotted in a Cartesian coordinate system linked to the microscope

stage. Z-coordinates are omitted in this presentation. Color represents time from NEB. **(A')** Same cell as in (A) but the trajectories are plotted in a spindle-centric cylindrical coordinate system comprising φ, angle to the horizon; ρ, distance to spindle axis; and z, distance to the equator. For convenience, in Axial views the sign of ρ coordinate is inverted for half of trajectories. This reduces crowding and the appearance of the plot resembles a spindle. Notice that most chromosomes remain near the equator throughout prometaphase. **(B,B')** Centromere trajectories in an untreated RPE1 cell shown from two viewpoints. Each trajectory is split into two segments – from NEB until the formation of amphitelic attachment on this centromere (B) and from the formation of amphitelic attachment until 900 sec after NEB (B'). Notice rapid linear movements of peripheral chromosomes towards the spindle axis prior to the formation of amphitelic attachment (B). Also notice that most chromosomes abruptly change direction of their movement and begin to move parallel to the spindle axis (B'). **(C)** Assessment of the dimensions of the biorientation domain in the wild type RPE1 cells. 1-d Gaussian functions are fit to the Axial and Equatorial distributions of centromere positions at the timepoint of amphitelic attachment formation and Full Width at Half Maximum (FWHM) of these fits calculated. Notice that both distributions are nearly normal $R^2 > 0.95$). **(D,D')** Similar to (B,B') but the cell is depleted of PRC1 (see Figure S2D). Notice that centripetal movements of centromeres prior to the formation of amphitelic attachment do not terminate abruptly but gradually convert into more regular movements along the spindle axis. **(E)** Similar to (C) but in PRC1-depleted RPE1 cells. Notice that changes in the Axial distribution are less prominent than in the Equatorial. The latter is not normal and positively skewed, indicating a high frequency of amphitelic attachment formations in at larger distances from the spindle axis.

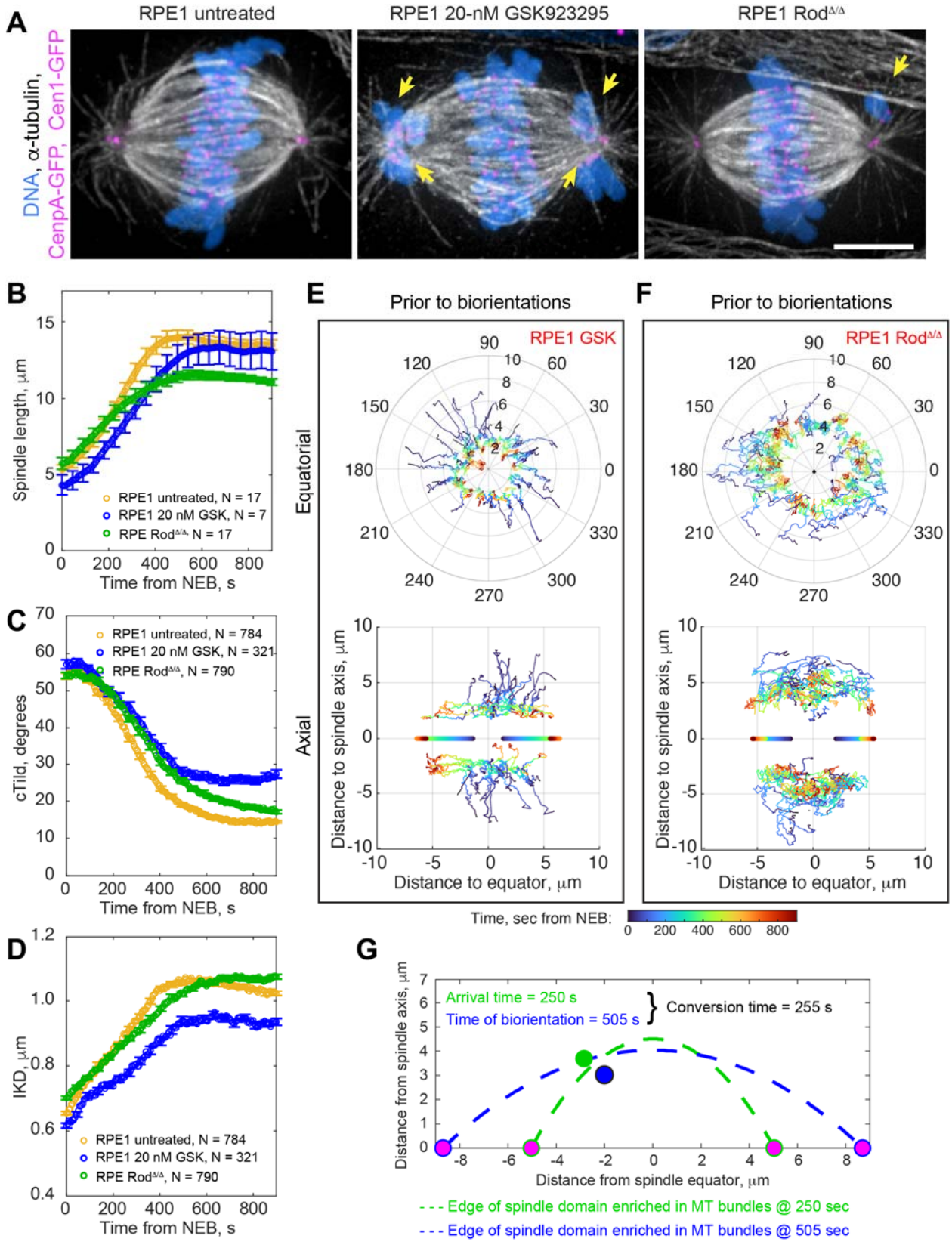
A
RPE1 untreated
RPE1 20-nM GSK923295
RPE1 Rod$^{\Delta/\Delta}$
DNA, α-tubulin,
CenpA-GFP, Cen1-GFP
B
Spindle length, μm
Time from NEB, s
RPE1 untreated, N = 17
RPE1 20 nM GSK, N = 7
RPE Rod$^{\Delta/\Delta}$, N = 17
C
cTild, degrees
Time from NEB, s
RPE1 untreated, N = 784
RPE1 20 nM GSK, N = 321
RPE Rod$^{\Delta/\Delta}$, N = 790
D
IKD, μm
Time from NEB, s
RPE1 untreated, N = 784
RPE1 20 nM GSK, N = 321
RPE Rod$^{\Delta/\Delta}$, N = 790
E
Prior to biorientations
RPE1 GSK
Equatorial
Axial
Distance to spindle axis, μm
Distance to equator, μm
F
Prior to biorientations
RPE1 Rod$^{\Delta/\Delta}$
Distance to spindle axis, μm
Distance to equator, μm
Time, sec from NEB:
G
Distance from spindle axis, μm
Arrival time = 250 s
Time of biorientation = 505 s
Conversion time = 255 s
Distance from spindle equator, μm
- - - Edge of spindle domain enriched in MT bundles @ 250 sec
- - - Edge of spindle domain enriched in MT bundles @ 505 sec

Figure S4. Spindle assembly and centromere trajectories in cells lacking CenpE- or dynein activity at the kinetochore. Related to Figure 6. (A) Principal components of the spindle during late prometaphase in the evaluated experimental conditions. Notice monooriented chromosomes (arrows) adjacent to spindle poles in cells with inhibited CenpE (RPE1 20-nM GSK923295) and in cells that lack dynein at the kinetochores (RPE1 $Rod^{\Delta/\Delta}$). Scale bar, 5 μm. **(B-D)** Dynamics of spindle elongation, cTilt, and IKD. Notice similar duration of spindle elongation in all three classes although the maximum length of the spindle in $Rod^{\Delta/\Delta}$ is significantly shorter than in the other two classes (B; $p < 0.001$ in Student's T-test). cTilt decreases at lower rates in CenpE-inhibited and $Rod^{\Delta/\Delta}$ cells (C). The final mean values reached 900 s after NEB are similar in the wild-type and $Rod^{\Delta/\Delta}$ RPE1 but is significantly higher in CenpE-inhibited cells (C). IKD increases significantly slower in CenpE-inhibited cells, and it plateaus at a lower lever in CenpE-inhibited cells (D; $p < 0.001$ in Student's T-test). Difference between the wild-type and $Rod^{\Delta/\Delta}$ RPE1 cells are not significant. Error bars, shown for every 10^{th} timepoint, are Standard Error of Mean. **(E,F)** Centromere trajectories prior to the formation of amphitelic attachments in a CenpE-inhibited (E) and in a $Rod^{\Delta/\Delta}$ RPE1 cell (F). Notice that rapid linear movements towards the spindle axis are present in CenpE-inhibited (E) but absent in $Rod^{\Delta/\Delta}$ cells (F). Also notice poleward movement of centromeres along the spindle axis during later stages of prometaphase (color-coded cyan to red) in (E, Axial) and during earlier stages of prometaphase (color-coded blue to cyan) in (F, Axial). **(G)** Methodology for assessing when a centromere is delivered to the biorientation domain, and the time required for the formation of amphitelic attachment within the domain. Green and blue dash lines are catenaries that mark the edge of the spindle domain enriched in microtubule bundles (Figure 4B and Methods) at two timepoints. Green dot denotes position of the centromere at the time point when the Euclidian distance to the contemporary catenary decreases to <0.85 μm for the first time. Blue dot denotes position of the same centromere when formation of amphitelic attachment is detected. Conversion time is the time lapsed from the arrival to amphitelic attachment formation.